Absolute and Relative-Rate Kinetics Experiments and Direct Dynamics Computations for the Reaction of Br Atoms with CH_2ClBr†

K. Imrik, Gg. Kovács, I. Fejes, I. Szilágyi, D. Sarzyński,‡ S. Dóbé,* T. Bérces,* and F. Márta

Chemical Research Center, Hungarian Academy of Sciences, Pusztaszeri út 59-67, Budapest H-1025, Hungary

J. Espinosa-García*

Departamento de Química Física, Universidad de Extremadura, 06071 Badajoz, Spain

Received: November 1, 2005; In Final Form: March 10, 2006

Kinetics of the reaction Br + CH_2ClBr ↔ CHClBr + HBr (1, −1) were studied experimentally in the forward direction. The absolute reaction kinetics method of laser flash photolysis coupled with Br atom resonance fluorescence detection and three different relative-rate methods with gas-chromatographic analysis were applied to carry out the experiments. The rate constants determined were found to obey the Arrhenius law in the wide temperature range of $T = 293-785$ K providing the kinetic expression $k_1 = (2.8 \pm 0.1) \times 10^{13} \exp[-(47.6 \pm 0.3)\ \text{kJ mol}^{-1}/RT]\ \text{cm}^3\ \text{mol}^{-1}\ \text{s}^{-1}$ (the errors given refer to 1σ precision). An ab initio direct dynamics method was used to study reaction (1, −1) theoretically. The electronic structure information including geometries, gradients, and force constants was obtained at the MP2 level of theory; and energies were improved at higher theoretical levels. Rate constants were calculated using the canonical variational transition state theory with small-curvature tunneling correction over the temperature range 200−1000 K. Theory substantially underestimates k_1 compared to experiment. The agreement was found good with k_{-1} reported previously predicting positive temperature dependence. The experimental kinetic parameters were utilized in thermochemical calculations yielding the recommended standard enthalpy of formation of $\Delta_f H^\circ_{298}$ (CHClBr) = (140 ± 4) kJ mol^{-1} (with 2σ accuracy given).

1. Introduction

Experimental and theoretical studies of the kinetics and dynamics of "bromination equilibrium reactions", such as reaction (1, −1), have been and continue to be the focus of research interest for several reasons.

$$\text{Br} + \text{CH}_2\text{ClBr} \leftrightarrow \text{CHClBr} + \text{HBr} \qquad (1, -1)$$

Bromine atoms are known to be highly effective in depleting the Earth's ozone layer through catalytic cycles.[1] The main source of Br is CH_3Br, but CH_2ClBr is also a permanent biogenic halocarbon that contributes to the bromine load of the atmosphere.[2−4] (Br without the spectroscopic term symbol designates ground-state Br($^2P_{3/2}$) atom throughout the paper.)

Experimental studies of the kinetics of equilibria involving the reactions of Br atoms with organic molecules have been a major source of thermochemical information on polyatomic free radicals for more than 60 years.[5−8] To add to this importance, the long-lasting debate continues in the chemical kinetics and dynamics literature on whether the reactions of hydrocarbon free radicals with HBr have positive or negative temperature dependence. (For recent developments of the debate see, e.g., refs 9−15.)

We have decided to study the kinetics of the reaction of Br atoms with CH_2ClBr (reaction 1) with the main objective to provide data for comparison with theory in a wide range of temperatures. A further motivation has been to determine a reliable enthalpy of formation value for the CHClBr radical by combining the kinetics information from the present study with that available for the reverse (−1) reaction.[16]

Both absolute and relative-rate (competitive-kinetics) methods are used in the experiments to be presented. We have found these methods to be essentially complementary to each other for the purpose of the present study. Reaction 1 is relatively slow for absolute techniques, and therefore the absolute kinetics measurements were carried out at elevated temperatures, while the relative-rate techniques were better suited for investigations at lower temperatures down to ambient.

In the present work, we perform a theoretical study of reaction (1, −1), i.e., in both directions. We first calculate the stationary point properties by using high level ab initio methods. In a second step, we apply theoretical information along the reaction path in a way which is usually referred to as a "direct dynamics" method.[17] This method describes a chemical reaction by using energies, gradients, and Hessians, "on the fly", along the reaction path. Such an approach has been successfully applied for several hydrogen abstraction reactions; see, e.g., refs 17−19. Finally, in a third step, we obtain kinetic information by performing variational transition-state theory (VTST) calculations with the inclusion of multidimensional tunneling effects (SCT).

To our knowledge, this is the first report of a combined experimental and direct dynamics study for a Br atom reaction.

† Part of the special issue "David M. Golden Festschrift".

* Corresponding authors. E-mail: dobe@chemres.hu (S.D.); joaquin@unex.es (J.E.-G.).

‡ Permanent address: Wrocław University of Medicine, Department of Chemistry, pl. Nankiera 1, 50-140 Wrocław, Poland.

10.1021/jp0563078 CCC: $33.50
Published on Web 04/07/2006

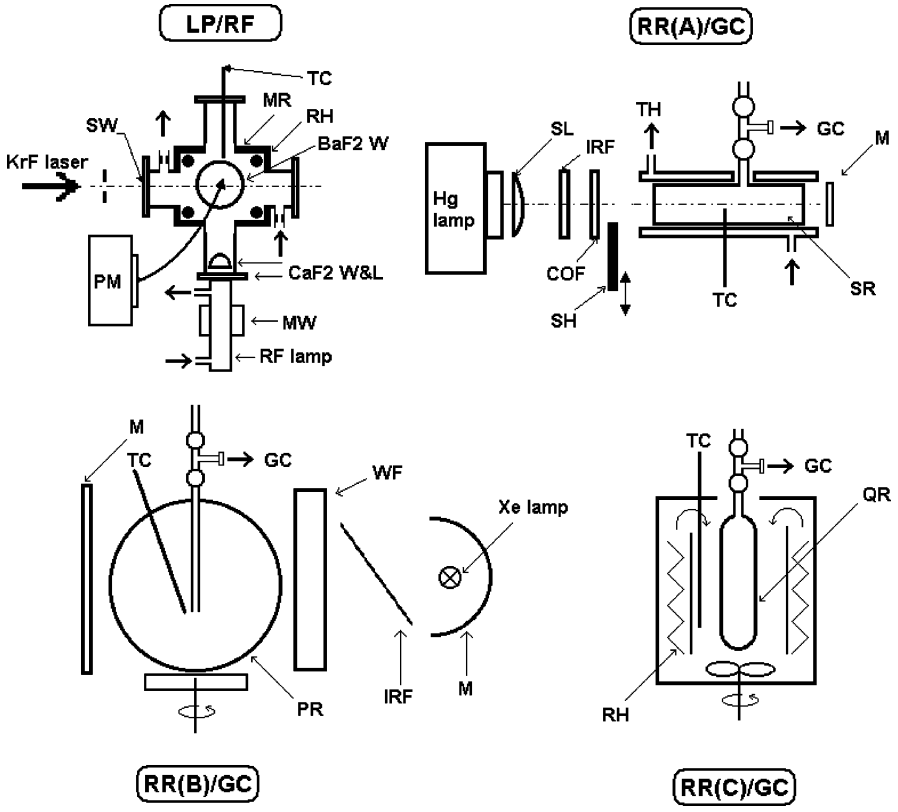

Figure 1. Schematic drawing of the experimental setups used for kinetic studies of the reaction of Br atoms with CH_2ClBr. LP/RF = laser flash photolysis/resonance fluorescence absolute kinetics method. RR(A)/GC = relative-rate method: photobromination with gas-chromatographic determination of products. RR(B)/GC = relative-rate method: photobromination with gas-chromatographic determination of the consumption of reactants. RR(C)/GC = relative-rate method: thermal bromination with gas-chromatographic determination of products. MR = metal reactor equipped with water-cooled window holders, SR = Suprasil reactor, PR = Pyrex reactor, QR = quartz reactor; SW = Suprasil window, BaF2W = BaF_2 window, CaF2W&L = CaF_2 window and CaF_2 lens, SL = Suprasil lens; IRF = infrared filter, COF = cutoff filter, WF = water filter; M = Al mirror; SH = shutter; GC = sampling port for GC analysis; RH = regulated resistance heating, TH = thermostat; TC = retractable thermocouple; PM = photomultiplier.

2. Experimental Section

Four experimental techniques were applied to study the kinetics of the reaction of Br atoms with CH_2ClBr. A schematic drawing of the experimental setups is presented in Figure 1. Figure 1 serves also to summarize some of the abbreviations used in the current paper.

2.1. Absolute Kinetics Technique. Laser flash photolysis (LP) coupled with time-resolved resonance fluorescence spectrometry of Br atoms (RF) was applied to determine absolute rate constants for reaction 1. The apparatus and methodology were very similar to those described previously.[20]

The reactor was constructed of stainless steel and heated electrically. A recently installed temperature controller provided stability of the reaction temperature within ± 0.5 K ($T \approx 750$ K). (The quoted uncertainties throughout this paper are 1σ of the measurement precision, unless otherwise stated, and do not include estimated systematic errors.) The reaction temperature was measured in the middle of the cell with a retractable shielded thermocouple. Optical windows were attached to the reactor through water-cooled, O-ring-sealed flanges.

The 248 nm exciplex laser photolysis of the reactant molecule CH_2ClBr proved to be a convenient source of Br atoms. The laser energy entering the reactor was kept low and changed by means of metal sieves when the CH_2ClBr concentration was varied in the kinetic experiments in order to maintain a small, approximately constant initial Br atom concentration ($[Br]_0 \approx (2-5) \times 10^{-13}$ mol cm^{-3}). In the present arrangement, the Br atom resonance fluorescence lamp, operated with flowing Br_2 (0.1%)/He through a microwave discharge, was attached directly to the reactor through a CaF_2 window. The induced Br atom resonance fluorescence ($\lambda \approx 160$ nm) was detected by a solar-blind PM at right angles to both the laser beam and the RF analytical light beam through a BaF_2 filter ($\lambda \geq 135$ nm). The BaF_2 filter prevented the possible impurity radiation of excited O and Cl atoms from entering the photomultiplier. Dry N_2 was flown in front of the PM tube to prevent absorption of the Br resonance fluorescence radiation by O_2.

The reaction mixtures were flown through the cell at a rate sufficient to replenish its content after four or five laser flashes so that the complications from product accumulation could be avoided. The main He flow and the CH_2ClBr flow, premixed ($\sim$10%) in helium, were regulated by an electronic mass flow controller and a needle valve, respectively. The concentration of CH_2ClBr was obtained by measuring its partial flow with the pressure-rise method and from the overall pressure in the reactor. Br atom fluorescence decay traces were captured by a digital storage oscilloscope and transferred to a PC for averaging and further analysis. Signals from 500−2000 laser shots were averaged to increase the signal-to-noise ratio. The detection limit for [Br] was less than 3×10^{-15} mol cm^{-3}.

The LP/RF technique was used at the highest temperature range of the investigations ($T = 699-785$ K).

2.2. Relative-Rate Techniques. In the relative-rate experiments rate constant ratios, k_1/k_2, were determined. The reference was the reaction of Br atoms with neopentane (2,2-dimethylpropane) for which absolute kinetic parameters are

available from our previous study.[21]

$$Br + neo\text{-}C_5H_{12} \rightarrow neo\text{-}C_5H_{11} + HBr \qquad (2)$$

Sources of Br atoms were either the stationary photolysis or the thermal decomposition of Br_2.

RR(A)/GC Method. Application of this method involved performing competitive photobromination experiments with CH_2ClBr/*neo*-C_5H_{12}/Br_2/He mixtures in combination with gas-chromatographic determination of the products $CHClBr_2$ and *neo*-$C_5H_{11}Br$. The experimental apparatus and procedure were similar to those described, e.g., in refs 22 and 23. The RR(A)/GC measurements were carried out at and above room temperature in ~120 K temperature interval.

The reactor was a cylindrical Suprasil cell of 150 cm^3 volume equipped with plane-parallel windows. It was surrounded by a thermostating oil jacket allowing the reaction temperature to be kept constant within ±0.2 K. Br_2/He and (CH_2ClBr + *neo*-C_5H_{12})/He mixtures were prepared manometrically in a conventional vacuum line and stored in large volumes. The reactants were admixed in the photolysis cell and were filled up to 1 bar with He. Irradiation was made by the parallel light beam of a high-pressure mercury arc. A 350 nm cutoff filter was applied to prevent the photodecomposition of the organic reactants and products while allowing the photolysis of Br_2. The irradiation time was varied from 1.5 to 180 min depending on the reaction temperature to keep the formation of the secondary bromination products as low as possible. The conversion of CH_2ClBr and *neo*-C_5H_{12} was always less than 7%. No dark reactions were observed even at the highest temperature photolytic experiments (T = 413 K). The reaction products were measured by isothermal (383 K) gas chromatography using a 3 m dinonyl-sebacate (10%)/Chromosorb W column and a flame ionization (FID) detector; N_2 was the carrier gas. The photolysis cell was equipped with a GC sampling port, which included a septum joint and could be evacuated separately. After irradiation, the sampling line was flashed through with the reaction mixture and samples for GC analysis were withdrawn by a gastight syringe. Measured peak areas were corrected for the relative sensitivities of the detector response that was accurately determined by calibrations with authentic samples.

RR(B)/GC Method. This is also a photolysis method, but in this case the consumption of the reactants, CH_2ClBr and *neo*-C_5H_{12}, was measured and compared. Similar experiments were described, e.g., by Bierbach et al.[24] The RR(B)/GC experiments were conducted in a 10 L Pyrex bulb, close to room temperature.

The reaction mixture, besides CH_2ClBr, *neo*-C_5H_{12}, and Br_2, contained also an inert gas-chromatographic internal standard, perfluoro-methyl-cyclohexane (c-C_7F_{14}), in order to determine the consumption of the organic reactants even at low conversions accurately. The organics and Br_2 were measured into the reactor manometrically, and the total reaction pressure was set to 1.0 bar with He.

For photolytic production of Br atoms, we used a modified movie projector, the light source of which was a 3 kW Xe arc. A parabolic reflector collimated the light of the Xe arc to a parallel beam of about 30 cm diameter. The IR component from the irradiating light beam was removed by means of a heat reflecting mirror in the lamp house and a water filter of 15 cm optical path length placed in front of the reactor. To maintain uniform reaction conditions in the irradiated mixture, the bulb was rotated with a speed of 16 rpm and a wall mirror was placed behind it. The reaction temperature was measured with a retractable thermocouple and was found constant, $T = 310 \pm 3$ K, in the whole reaction volume. The photolysis time was varied between 20 and 300 min, and the conversion of the reactants was in the range of 6−55%.

Samples for analysis were withdrawn by a gastight syringe through a septum connected to a glass capillary tube which reached in the center of the bulb. The dead volume of the sampling line was evacuated and flushed before sampling.

The concentrations of the organic reactants were determined by temperature programmed gas chromatography using a 3 m Porapak P column and FID. Calibrations against the internal standard were accomplished with gas samples of known composition.

RR(C)/GC Method. The source of Br atoms was the thermal decomposition of Br_2, and here again products were measured by GC. The 180 cm^3 cylindrical reactor was made of fused silica. It was placed in an electric oven, in which forced air circulation provided uniform temperature within ±0.5 K. The temperature was regulated by means of a feedback system the sensing element of which was a Pt resistance thermometer. The transient temperature regimes were minimized by using capillary tubing in the gas-filling/sampling lines. Also, the reaction components were premixed and preheated to 413 K in a separate volume before entering the reactor. Gas-chromatographic analyses were done as described above for RR(A)/GC. The temperature range was the closest to that of the LP/RF investigations but not yet overlapping (T = 435−583 K).

Materials. He (99.996%, Messer-Hungaria) was used as provided. CH_2ClBr (99%, Aldrich), *neo*-C_5H_{12} (99%, Fluka), $CHClBr_2$ (98%, Aldrich), *neo*-$C_5H_{11}Br$ (98%, Aldrich), and c-C_7F_{14} (97%, Fluka) were degassed by freeze−pump−thaw cycles prior to use. Br_2 (99+%, Aldrich) was stored over KBr and subjected to several low-temperature trap-to-trap distillations to remove traces of Cl_2.

3. Computational Method

3.1. Ab Initio Calculations. Molecular orbital calculations were carried out using the GAUSSIAN 98 system of programs.[25] The geometrical parameters were fully optimized at the second-order Møller−Plesset perturbation (MP2) theoretical level[26] with full electron correlation using the 6-31G(d,p) basis set. Singlet states (molecules) and doublet states (radicals) were calculated applying the restricted version (R) and the unrestricted version (U) of the theory, respectively. This is our level 0 ((R-U)MP2=FULL/6-31G(d,p)).

At this MP2/6-31G(d,p) level we have constructed the "intrinsic reaction coordinate" (IRC), or minimum energy path (MEP), starting from the saddle point geometry and going downhill to both the asymptotic reactant and product valleys in mass-weighted Cartesian coordinates with a gradient step size of 0.02 bohr $amu^{1/2}$. Along this MEP, the reaction coordinate, s, is defined as the signed distance from the saddle point, with $s < 0$ referring to the Br + CH_2ClBr reactants' side. In the present work, s is given in bohr, and the reduced mass to scale the coordinates[27] is set to 1 amu. Moreover, both the harmonic vibrational frequencies and the reaction path curvature components were computed each two points along the reaction path in the range $s = \pm 1$ bohr.

In a second step, in order to obtain more reliable reaction energy and barrier height, we have performed single-point energy calculations at higher theoretical levels:

Level I. In this case single-point calculations were carried out at the fourth order of Møller−Plesset perturbation theory with the frozen-core approximation and single, double, triple, and quadruple replacements (MP4SDTQ), using the

6-311G(3d,2p) basis set. The energy obtained in this way is denoted by

(R-U)MP4SDTQ/6-311G(3d,2p)//
(R-U)MP2=FULL/6-31G(d,p)

This approach presents two problems. First, it is well-known that MP perturbation theory converges slowly, especially in the case of free radicals.[28,29] Second, as the UHF wave function is not necessarily an eigenfunction of the S^2 operator, we find spin contamination in the radicals. The saddle point presents the largest expectation value of S^2: 0.786 at the UMP2/6-31G(d,p) level. This contamination was corrected by use of projecting operators as implemented in GAUSSIAN 98.[25] The energy after the spin decontamination will be PMPn (projected MPn).

Level II. The procedure applied here corresponds to single-point calculations of the total electronic energy by means of single and double coupled cluster theory with inclusion of a perturbative estimate for triple excitations,[30] CCSD(T), using the 6-311G(d,p) basis set. We denote this energy as

CCSD(T)/6-311G(d,p)//(R-U)MP2=FULL/6-31G(d,p)

Level III. Gaussian-2 (G2) Theory. The G2 theory is based on a combination of ab initio calculations and is described fully in the original paper.[31] In brief, it uses structures optimized at the MP2/6-31G(d) level and energies calculated at the MP4/6-311G(d,p) level and augmented by corrections for diffuse functions, a correction for higher polarization functions, a correction for correlation effects beyond fourth-order perturbation theory, and an empirical higher-level correction to account for remaining basis set deficiencies. Although G2 was not specifically designed to compute reaction transition states, the performance of this method was found remarkably good for different classes of reactions.[32,33] The classical barrier heights for the studied reactions were predicted with an absolute average deviation of about 6 kJ mol^{-1}, but the G2 method was concluded less successful in predicting geometries and frequencies.[32,33]

3.2. Direct Dynamics Calculations. We have performed a generalized normal-mode analysis projecting out frequencies at each point along the MEP.[34] With this information, we have calculated, first, the ground-state vibrationally adiabatic potential curve

$$V_a^G(s) = V_{MEP}(s) + \epsilon_{int}^G(s) \quad \text{(I)}$$

where $V_{MEP}(s)$ is the classical energy along the MEP with its zero at the reactants ($s = -\infty$), and $\epsilon_{int}^G(s)$ is the zero-point energy at s from the generalized normal-mode vibrations orthogonal to the reaction coordinate. As a second step, the coupling terms, $B_{k,F}(s)$, were computed. The $B_{k,F}(s)$ terms quantify the coupling between the normal mode, k, and the motion along the reaction coordinate, mode F. They control the nonadiabatic flow of energy[35,36] allowing us to calculate accurate semiclassical tunneling factors, i.e., dynamical features. The coupling terms are also components of the reaction path curvature, $\kappa(s)$, defined as

$$\kappa(s) = \left(\sum [B_{k,F}(s)]^2\right)^{1/2} \quad \text{(II)}$$

Finally, the energies, vibrational frequencies, geometries, and gradients along the MEP were used to estimate rate constants by using variational transition state theory (VTST). We calculated thermal rates using the canonical variational theory[37,38] (CVT) approach which locates the dividing surface between reactants and products at a point $s^{*,CVT}(T)$ along the reaction path that minimizes the generalized TST rate constants, $k^{GT}(T,s)$, for a given temperature, T. Thermodynamically, this is equivalent to locating the transition state at the maximum $\Delta G^{GT,\circ}[T,s^{*,CVT}(T)]$ of the standard-state free energy of activation profile $\Delta G(T,s)$.[37,38] Thus, the thermal rate constant will be given by

$$k^{CVT}(T) = \sigma \frac{k_B T}{h} K^\circ \exp[\Delta G^{GT,\circ}(T,s^{*,CVT})/k_B T] \quad \text{(III)}$$

where k_B is Boltzmann's constant, h is Planck's constant, σ is the reaction degeneracy (the number of equivalent reaction paths, which were taken 2 and 1 for the forward and reverse reactions, respectively), and K° is the reciprocal of the standard-state concentration, taken as 1 mol cm^{-3} (we note, however, that all thermochemical quantities reported in our paper refer to the usual 1 bar standard state).

As a last step, we consider the tunneling contribution. Since we have information only on the reaction path, the centrifugal-dominant small-curvature tunneling (SCT)[39,40] approximation is used.

All kinetics and dynamics calculations were carried out with the general polyatomic rate constant code POLYRATE.[40]

4. Experimental Results

4.1. Rate Constants for Reaction 1. *LP/RF Results.* The absolute kinetics experiments were carried out at $T = 699-785$ K reaction temperature and pressures in the range of $P = 160-215$ mbar, in He buffer gas. The bimolecular rate constant, k_1, was determined by the usual pseudo-first-order experimental approach of monitoring the concentration−reaction time ([Br]/t) profiles after laser flashes in the presence of a large excess of the reactants, $[CH_2ClBr] \gg [Br]_0$; $[CH_2ClBr]/[Br]_0 > 10^5$.

In the absence of interfering parallel or consecutive reactions, which significantly consume or re-form the Br atoms, the decay of Br concentration is given by the simple rate expression

$$[Br]_t/[Br]_0 = I_t/I_0 = \exp(-k_1' t) \quad \text{(IV)}$$

$$k_1' = k_1[CH_2ClBr] + k_d \quad \text{(V)}$$

where $[Br]_0$ and $[Br]_t$ are the concentrations of Br at times zero and t, respectively, I_0 and I_t are the corresponding resonance fluorescence signal strengths, k_1' is the measured pseudo-first-order rate (decay) constant, and k_d is the first-order rate constant for removal of Br in the absence of CH_2ClBr and is primarily attributed to diffusion out of the detection volume.

The temporal profile of [Br] followed a single-exponential decay in all experiments according to eq IV. Nonlinear least-squares analysis was applied to obtain the pseudo-first-order rate constants at different temperatures. The fitting procedure supplied the k_1' parameters with small errors that were taken equal in further analyses. Plots of the pseudo-first-order rate constants vs $[CH_2ClBr]$ yielded the bimolecular rate constants as linear least squares slopes. Representative examples of such plots are presented in Figure 2. The intercepts provided $k_d = (47 \pm 7)$ s^{-1} with slight increase with temperature within the given range. The experimental conditions applied, and the kinetic results obtained have been summarized in Table 1. Observation of a linear dependence of k_1' on $[CH_2ClBr]$ and invariance of k_1 to variations in $[Br]_0$ (see Table 1) serve as arguments that no significant systematic errors due to secondary chemistry were involved in the measurements. The possible systematic errors were assessed by further investigations below:

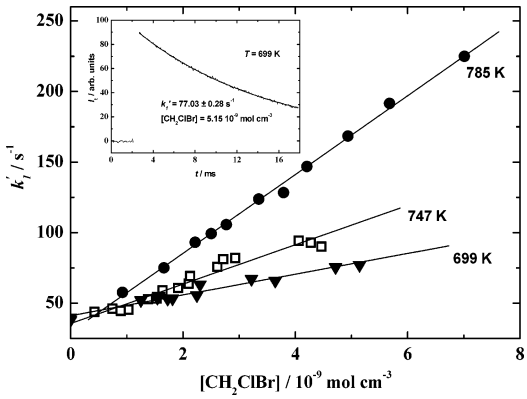

Figure 2. Representative plots of pseudo-first-order rate constant vs the CH_2ClBr concentration obtained from LP/RF absolute kinetics experiments. The inset shows a typical Br atom resonance fluorescence decay with a single-exponential fit to the experimental data.

TABLE 1: Summary of Experimental Conditions and Kinetic Results for the LP/RF[a] Experiments[b]

T (K)	$[CH_2ClBr]$ (10^{-9} mol cm^{-3})	k_1' (s^{-1})	$[Br]_0$ (10^{-13} mol cm^{-3})	k_1 (10^{10} cm^3 mol^{-1} s^{-1})	N_{exp}[c]
699 ± 3	1.3−5.2	52−77	1.7−6.7	0.80 ± 0.05	12
714 ± 1	1.1−4.2	45−73	1.2−8.6	0.89 ± 0.07	10
722 ± 1	1.5−7.8	48−121	1.3−9.6	0.94 ± 0.07	18
732 ± 1	0.6−6.6	44−109	0.8−3.8	1.01 ± 0.10	16
747 ± 1	0.4−8.5	44−137	3.5−21.5	1.34 ± 0.05	16
758 ± 4	1.2−7.6	58−152	1.3−8.3	1.49 ± 0.10	17
785 ± 3	1.0−5.7	54−170	1.7−5.3	1.85 ± 0.15	12

[a] Laser flash photolysis/resonance fluorescence absolute reaction kinetics method. [b] Errors are 1σ statistical uncertainties. [c] Number of experiments.

Br reacts relatively slowly with CH_2ClBr, and so reactive impurities even in small concentration might have caused an overestimation of k_1. Thus, we have analyzed the purity of the CH_2ClBr sample by GC on three different-polarity columns: no impurities could be detected.

In the LP/RF experiments the source of ground-state bromine atoms was the laser photolysis of CH_2ClBr: $CH_2ClBr + h\nu$(248 nm) → $Br(^2P_{3/2})$ + CHClBr. Energetically it is possible that spin−orbit-excited $Br(^2P_{1/2})$ (hereafter designated as Br*) and ground-state $Cl(^2P_{3/2})$ atoms might also be produced at this wavelength. In a detailed photodissociation-dynamics experimental study, McGivern and co-workers[41] have shown, however, that practically only the ground-state $Br(^2P_{3/2})$ is formed. In a test experiment, we could not detect Cl atoms for the 248 nm photolysis of CH_2ClBr by using the Cl atom resonance fluorescence detection technique.

The lowest applicable reaction temperature was explored by trial experiments conducted between 633 and 683 K. Very high concentrations of CH_2ClBr had to be used which involved a high initial concentration of Br atoms and therefore an overestimation of k_1 in this temperature range. The highest temperature accessible for quantitative kinetic studies was limited by the thermal decomposition of CH_2ClBr that probably occurred on the hot surface of the metal reactor.

The temperature dependence of the rate constant for the reaction Br + CH_2ClBr (1) can be described by the Arrhenius expression of $k_1 = (5.0 \pm 0.5) \times 10^{13} \exp[(-51.2 \pm 0.6 \text{ kJ mol}^{-1})/RT)]$ cm^3 mol^{-1} s^{-1} ($T = 699-785$ K) by results of the LP/RF absolute kinetics experiments. (The Arrhenius parameters in this work have been obtained by nonlinear least-squares analysis of the experimental data with N_{exp}/σ_i^2 weighting.)

RR(A)/GC and RR(C)/GC Results. The essence of the two experimental methods is the same, competitive bromination with measurement of products; therefore the results obtained with them are presented together although the way of production of Br atoms was different.

The RR(A)/GC photobromination experiments were carried out at $T = 293-413$ K and the RR(C)/GC thermal brominations between 435 and 583 K both in 1.0 bar of He. The experimental conditions and results are given in Table 2.

The reaction systems studied are described by the following reaction mechanism:

$$Br_2 + h\nu \text{ or } \Delta \rightarrow 2Br \qquad \text{(initiation)}$$

$$Br + CH_2ClBr \leftrightarrow CHClBr + HBr \qquad (1, -1)$$

$$Br + neo\text{-}C_5H_{12} \leftrightarrow neo\text{-}C_5H_{11} + HBr \qquad (2, -2)$$

$$CHClBr + Br_2 \rightarrow CHClBr_2 + Br \qquad (3)$$

$$neo\text{-}C_5H_{11} + Br_2 \rightarrow neo\text{-}C_5H_{11}Br + Br \qquad (4)$$

In analogy with the reactions of other carbon-centered free radicals with Br_2,[42,43] reactions 3 and 4 are likely to be fast. Thus, at the long reaction chains and for low conversions with respect to the organic reactants, the reverse reactions −1 and −2 can be neglected[6] and rate constant ratios are related to the measured product concentration ratios by the simple equation

$$k_1/k_2 = ([CHClBr_2] \times [neo\text{-}C_5H_{11}]_0)/([neo\text{-}C_5H_{11}Br] \times [CH_2ClBr]_0) \qquad \text{(VI)}$$

where the subscript 0 designates initial concentration.

The validity of eq VI was tested over a range of bromine concentrations, $[CH_2ClBr]_0/[neo\text{-}C_5H_{11}]_0$ ratios, and photolysis times, and the k_1/k_2 ratios were found invariant to these changes at a given reaction temperature. No dark reaction could be observed even for the highest temperature photolytic experiments ($T = 413$ K).

The rate constant ratios were placed on the absolute scale by taking the rate constant expression for the reference reaction Br + $neo\text{-}C_5H_{12}$ (2) from ref 21, i.e., $k_2 = (6.9 \pm 2.3) \times 10^{14} \exp[(-57.6 \pm 2.1 \text{ kJ mol}^{-1})/RT]$ cm^3 mol^{-1} s^{-1} ($T = 688-775$ K). The derived k_1 values, with propagated errors, are listed in Table 2.

The temperature dependence of reaction 1 has been found to obey the Arrhenius expression by the relative-rate measurements as well with the kinetic parameters of $A_1 = (3.4 \pm 2.2) \times 10^{13}$ cm^3 mol^{-1} s^{-1} and $E_{A,1} = (47.4 \pm 2.0)$ kJ mol^{-1} ($T = 293-413$ K, RR(A)/GC) and $A_1 = (2.1 \pm 2.4) \times 10^{13}$ cm^3 mol^{-1} s^{-1} and $E_{A,1} = (45.4 \pm 5.2)$ kJ mol^{-1} ($T = 435-583$ K, RR(C)/GC).

RR(B)/GC Results. These are the results from our "big-bulb" photobromination experiments when the depletion of the organic reactants was determined at different reaction times (t). Provided that CH_2ClBr and $neo\text{-}C_5H_{12}$ reacted only with Br atoms as expected for the experimental conditions employed (see in Table 2), then

$$\ln([CH_2ClBr]_0/[CH_2ClBr]_t) = (k_1/k_2)\ln([neo\text{-}C_5H_{11}]_0/[neo\text{-}C_5H_{11}]_t) \qquad \text{(VII)}$$

Thus, a plot of $\ln([CH_2ClBr]_0/[CH_2ClBr]_t)$ against $\ln([neo\text{-}C_5H_{11}]_0/[neo\text{-}C_5H_{11}]_t)$ should be a straight line with slope of k_1/k_2 and an intercept of zero. The data obtained from several

TABLE 2: Summary of Experimental Conditions and Kinetic Results for the Relative-Rate (RR) Experiments[a] (P = 1.0 bar of He)

T (K)	$[CH_2ClBr]_0$ (10^{-7} mol cm^{-3})	$[neo\text{-}C_5H_{12}]_0$ (10^{-7} mol cm^{-3})	$[Br_2]_0$ (10^{-7} mol cm^{-3})	k_1/k_2[b]	k_1[c] (cm^3 mol^{-1} s^{-1})	N_{exp}[d]
			RR(A)/GC[e] Results			
293 ± 3	8.19−16.38	2.73−5.46	1.97−2.73	3.30 ± 0.10	(1.21 ± 1.14) × 10^5	4
312.0 ± 0.2	8.19−13.11	2.73−4.37	1.64−3.28	2.56 ± 0.11	(3.99 ± 3.59) × 10^5	4
323.0 ± 0.2	8.19−13.11	2.73−4.37	1.64−2.73	2.16 ± 0.02	(7.17 ± 6.03) × 10^5	4
333.0 ± 0.2	5.08−13.11	1.69−4.37	1.64−2.73	2.00 ± 0.04	(1.27 ± 1.05) × 10^6	5
343.0 ± 0.2	8.19−13.11	2.73−4.37	2.18−2.73	1.74 ± 0.08	(2.02 ± 1.69) × 10^6	3
345.0 ± 0.2	8.19−11.47	2.73−3.82	1.64−2.73	1.71 ± 0.08	(2.23 ± 1.86) × 10^6	4
355.0 ± 0.5	8.19−9.83	2.73−3.28	1.64−2.73	1.45 ± 0.03	(3.33 ± 2.63) × 10^6	3
373.0 ± 0.5	6.56−8.19	2.18−2.73	1.64−2.18	1.28	(7.54 ± 5.87) × 10^6	2
383.0 ± 0.5	8.19	2.73	2.18	1.11	(1.06 ± 0.82) × 10^7	1
393.0 ± 0.5	8.20	2.73	2.18−2.73	0.99 ± 0.11	(1.50 ±1.23) × 10^7	3
413.0 ± 0.5	6.56−8.19	2.18−2.73	1.64−2.73	1.04 ± 0.01	(3.70 ± 2.56) × 10^7	4
435.0 ± 0.5	6.56−8.19	2.18−2.73	1.64−2.73	0.9	(7.49 ± 5.24) × 10^7	2
			RR(B)/GC[f] Results			
310 ± 3	0.242−0.489	0.081−0.163	0.807−1.42	2.61 ± 0.05	(3.53 ± 3.10) × 10^5	17
			RR(C)/GC[g] Results			
465.0 ± 0.5	10.33	3.44	2.75	0.74	(1.72 ± 1.14) × 10^8	2
483.5 ± 0.5	4.97−7.95	1.66−2.65	1.66	0.58	(2.35 ± 1.51) × 10^8	3
503.0 ± 0.5	4.77−5.73	1.59−1.91	1.27−1.59	0.58 ± 0.01	(4.16 ± 2.53) × 10^8	3
523 ± 1	4.59	1.53	1.53	0.52 ± 0.03	(6.31 ± 4.00) × 10^8	3
543 ± 1	3.53−5.31	1.18−1.77	0.88−1.47	0.45 ± 0.03	(8.90 ± 5.59) × 10^8	5
583 ± 1	3.29	1.10	0.82−1.37	0.37	(1.76 ± 1.04) × 10^9	3

[a] Errors are 1σ statistical uncertainties. [b] Reference reaction: Br + *neo*-C_5H_{12} (2). [c] The rate constant ratios have been resolved by the absolute Arrhenius parameters reported in ref 21 for reaction 2. [d] Number of experiments. [e] Photobromination with gas-chromatographic determination of products. [f] Photobromination with gas-chromatographic determination of the consumption of reactants. [g] Thermal bromination with gas-chromatographic determination of products.

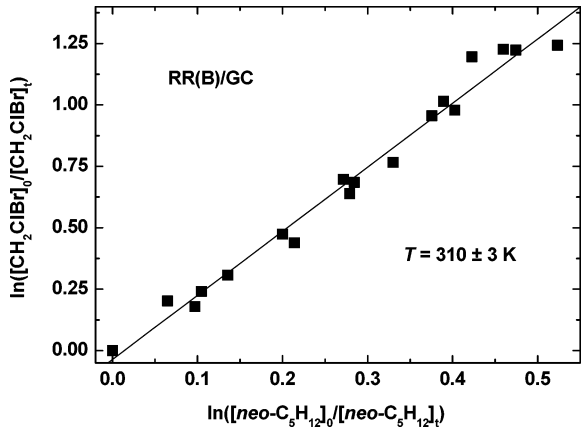

Figure 3. Plot used to determine the rate constant ratio k_1/k_2 from RR(B)/GC photobromination experiments at T = (310 ± 3) K.

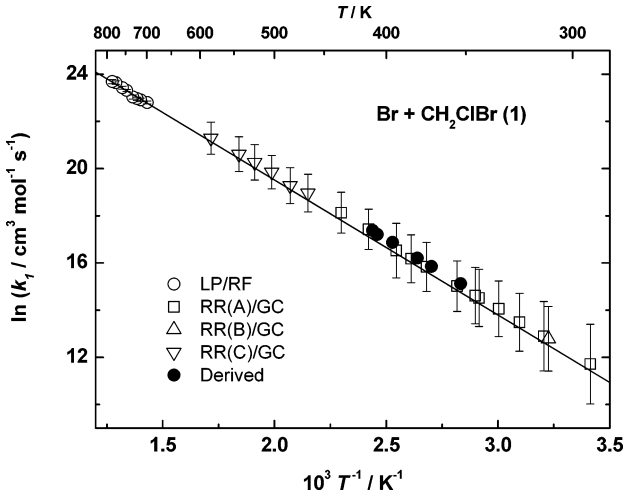

Figure 4. Temperature dependence of the rate constant for reaction 1 by results from absolute and relative-rate kinetics experiments. Data designated with filled circles have been derived by kinetic and thermochemical parameters reported in the literature (see text).

irradiations are plotted in accordance with eq VII in Figure 3. Least-squares analysis of the data yields the rate constant ratio k_1/k_2 = 2.64 ± 0.05 (T = 310 K) with an intercept of zero within the experimental uncertainties (the intercept is −0.04 ± 0.06(2σ)). This rate constant ratio agrees well with k_1/k_2 = 2.56 ± 0.11 (T = 312 K) that was obtained by applying the RR(A)/GC method (see above).

Temperature Dependence of k_1. The rate constants determined with the different experimental methods are presented as a plot of ln k_1 vs $1/T$ in Figure 4. The temperature dependence is described very well by a straight line providing the recommended rate constant expression from our current experimental study:

$$k_1 = (2.8 \pm 0.1) \times 10^{13} \exp[(-47.6 \pm 0.3)\ \text{kJ mol}^{-1}/RT]\ \text{cm}^3\ \text{mol}^{-1}\ \text{s}^{-1} \quad (T = 293-785\ \text{K})$$

4.2. Enthalpy of Formation for the CHClBr Radical. The kinetic results obtained for the reaction between bromine atom and CH_2ClBr (reaction 1), together with the kinetic data for the reverse reaction CHClBr + HBr (reaction −1),[16] have been used to determine the standard enthalpy of formation for the CHClBr radical, $\Delta_f H°_{298}$(CHClBr). (For a detailed example of deriving thermochemical data from kinetic results by using second law and third law methods, see, e.g., ref 20).

The kinetics of reaction −1 were investigated by Seetula[16] applying laser flash photolysis in a heatable tubular reactor coupled to a photoionization mass spectrometer (LP/PIMS). From measurements performed in the wide temperature range of 414−787 K, he has proposed the rate equation of k_{-1} = (3.0 ± 0.7) × 10^{11} exp[−(8.2 ± 0.3) kJ mol^{-1}/RT] cm^3 mol^{-1} s^{-1}.

In the second law derivation, the enthalpy change in reaction 1 is taken as the difference of the activation energies for the forward and reverse reactions at the mean temperature, 600 K,

of the overlapping temperature ranges, from which the standard reaction enthalpy of

$$\Delta_r H^\circ_{298}(1) = (40.4 \pm 0.4)\ \text{kJ mol}^{-1}$$

is obtained by using tabulated enthalpy increments[44] (the standard state refers to 1 bar and 298.15 K). The reaction enthalpy is resolved to

$$\Delta_f H^\circ_{298}(\text{CHClBr}) = (140.4 \pm 2.0)\ \text{kJ mol}^{-1}$$

by making use of the ab initio value of $\Delta_f H^\circ_{298}(CH_2ClBr) = (-48.1 \pm 2.5)$ kJ mol^{-1} from Espinosa-García and Dóbé[45] (see Discussion) and other auxiliary enthalpies of formation.[44]

In the third law calculation, the free energy change for the reaction has been obtained from the equilibrium constant, $K_1 = k_1/k_{-1}$, at the medium temperature of $T = 600$ K yielding $\Delta_r G^\circ_{600}(1) = -RT \ln K_1 = (16.7 \pm 1.23)$ kJ mol^{-1}. Temperature correction to 298 K is done by means of auxiliary enthalpy[44,45] and entropy[46] data providing the third law enthalpy of formation value of

$$\Delta_f H^\circ_{298}(\text{CHClBr}) = (136.7 \pm 2.8)\ \text{kJ mol}^{-1}$$

The agreement between the second law and third law results is acceptable; we prefer, however, the second law value for reasons given in section 6.1.

5. Computational Results

5.1. Structural Parameters and Vibrational Frequencies. On tracing the minimal energy path, we have located the following stationary structures at the MP2=FULL/6-31G(d,p) theoretical level: one hydrogen bonded complex (RHB) formed between the reactants Br and CH_2ClBr, the reaction saddle point (SP), and one hydrogen bonded complex (PHB) formed between the products CHClBr and HBr. The RHB and PHB complexes are minima on the potential energy surface with eigenvalues of the Hessian matrix that are all positive. The saddle point has one negative eigenvalue and, therefore, one imaginary frequency associated with the breaking and forming bonds. The geometrical parameters and harmonic vibrational frequencies for all stationary points are summarized in Table 3. It is well-known that MP2 theory overestimates the vibrational frequencies; therefore the computed values were scaled by 0.95.[47] The theoretical structural parameters and vibrational frequencies agree reasonably well with the scarce experimental data available[48,49] (see in Table 3).

The RHB complex was located on the PES with a Br···H distance of 2.926 Å. The C−H stretching frequency is practically unchanged compared with that in the CH_2ClBr molecule, which may question the real existence of this complex. The saddle point properties show characteristics of a "late" transition state. This is the expected behavior that would follow from Hammond's postulate since the Br + CH_2ClBr (1) reaction is significantly endothermic. The length of the C−H bond that is being broken increases by 35%, while the length of the H−Br bond that is being formed is larger by only 9% with respect to the CH_2ClBr and HBr molecules, respectively. The PHB complex has a C···H bond length of 2.469 Å and a C···H···Br angle of 180°. The lowest frequencies for this product's complex exhibit extremely small values which suggest a very flat surface. In the PHB complex we find that the stretching frequency of HBr (2773 cm^{-1}) is shifted to lower frequency by 43 cm^{-1}, and it increases in intensity from 9.4 to 154.0 km mol^{-1}. This is the expected behavior of a typical hydrogen bonded system.

TABLE 3: Structural Parameters and Vibrational Frequencies for Reactants, Products, Saddle Point and Hydrogen Bonded Complexes for Reaction (1, −1)[a]

Parameter[b]	CH_2ClBr[c]	CHClBr[d]	HBr[e]	RHB[f]	SP[g]	PHB[h]
			Geometry			
R1 (R_{HBr})			1.404	2.926	1.531	1.407
R2 (R_{CH})	1.082			1.083	1.466	2.469
R3 (R_{CH})	1.082	1.077		1.082	1.083	1.078
R4 (R_{CCl})	1.759	1.700		1.758	1.708	1.697
R5 (R_{CBr})	1.942	1.869		1.941	1.881	1.868
α				111.4	100.2	108.7
β				180.0	175.9	180.0
γ ($\angle$ClCBr)	109.2	116.6				
δ ($\angle$HCBr)	106.8	115.7				
			Frequency			
	3310	3324	2773	3313	3263	3317
	3218	1284		3220	1276	2730
	1517	900		1527	1082	1281
	1316	700		1332	913	902
	1210	543		1221	887	705
	886	256		900	825	575
	797			800	712	257
	632			633	413	232
	239			239	252	104
				91	109	89
				29	53	45
				10	914i	17
			TC			
	9.6	9.6	6.3	13.8	14.2	17.6
			ZPE			
	78.7	41.8	16.7	79.5	58.6	60.7

[a] Computed at the (R-U)MP2=FULL/6-31G(d,p) level. [b] Distances are given in angstroms, angles in degrees, frequencies in cm^{-1}, thermal corrections for 298 K (TC) and zero-point energies (ZPE) in kJ mol^{-1}. [c] Experimental bond distances: $R_{CH} = 1.115$ Å (assumed), $R_{CBr} = 1.928$ Å, $R_{CCl} = 1.755$ Å, $\angle$HCBr = 109.3° (ref 71). [d] Experimental frequencies: 1196, 866 cm^{-1} (ref 49). [e] Experimental values: $R_{HBr} = 1.414$ Å, frequency 2649 cm^{-1} (ref 48). [f] Hydrogen bonded complex formed between the reactants, Br and CH_2ClBr. [g] Reaction saddle point. [h] Hydrogen bonded complex formed between the products, CHClBr and HBr.

5.2. Relative Energies and Reaction-Path Analysis. The electronic energy changes, ΔE, and the enthalpy changes, ΔH°_0 and ΔH°_{298}, are listed in Table 4 estimated at the theoretical levels 0−III. Note that ΔH°_0 is the ΔE corrected for zero-point energy, and ΔH°_{298} includes the thermal correction to 298 K. Their accuracy depends on several factors: level of calculation (correlation energy + basis set), spin projection, quality of the thermal corrections, basis set superposition error, and spin−orbit (s−o) coupling. In order to facilitate the discussions below, the zeros of energies and enthalpies have been chosen as follows: RHB, relative to reactants Br + CH_2ClB; SP and PHB, relative to products, CHClBr + HBr.

We analyze first the reaction enthalpies because this may give an insight to the different factors that affect the accuracy of the theoretical results. A direct comparison of theory with experiment is not possible for the reaction Br + CH_2ClBr ↔ CHClBr + HBr (1, −1) because it is well-known that relativistic effects have to be included in theoretical calculations with heavy atoms due to s−o coupling[50] and an exhaustive relativistic study is beyond the scope of this work. As an approximation to include the s−o effect, one-third of the energy splitting between the $J = 1/2$ and $J = 3/2$ states of ^{2}P atomic bromine have been added to the theoretical reaction enthalpies.[51,52] Thus, the corrected theoretical reaction enthalpy, $\Delta_r H^{corr}$, is obtained from the expression

$$\Delta_r H^{corr} = \Delta_r H^{theo} + (1/3)[E(^2P_{1/2}) - E(^2P_{3/2})]$$

TABLE 4: Relative Energies and Enthalpies Computed at Different Theoretical Levels[a]

level[b]	RHB[c]	SP[d]	PHB[e]	(CHClBr + HBr)[f]
		ΔE^g		
0	−4.2	5.0	−11.7	58.2
I	0.4	−2.1	−9.2	54.0
II	1.7	11.3	−5.0	55.7
III	3.3	2.9	−1.3	46.5
		$\Delta H°_0{}^h$		
0	−2.9	5.0	−9.2	38.1
I	1.7	−2.1	−6.7	34.3
II	2.5	11.3	−2.9	35.6
III	0.4	4.2	−4.6	28.9
		$\Delta H°_{298}{}^i$		
0	−5.0	3.8	−7.5	38.1
I	−0.4	−3.8	−5.0	34.3
II	0.4	10.0	−1.3	35.6
III	0.8	0.4	−3.8	31.8

[a] Values are given in kJ mol^{-1} and do not include correction for s−o effect. [b] Level 0: MP2 theory. Level I: PMP4 theory. Level II: CCSD(T) theory. Level III: G2 theory. [c] Hydrogen bonded complex formed between the reactants Br and CH_2ClBr. Energies and enthalpies are given relative to reactants. [d] Reaction saddle point. Energies and enthalpies are given relative to products, CHClBr + HBr. [e] Hydrogen bonded complex formed between the products CHClBr and HBr. Energies and enthalpies are given relative to products. [f] Energies and enthalpies are given relative to reactants, Br + CH_2ClBr. [g] Electronic energy change. [h] Enthalpy change at $T = 0$ K. [i] Enthalpy change at $T = 298$ K.

where it is assumed that s−o effects are completely quenched in molecules. The two low-lying electronic states of bromine atom, $^2P_{1/2}$ and $^2P_{3/2}$, are separated by 3685.2 cm^{-1} (ref 48), and, therefore, the correction for $\Delta_r H^{\text{theo}}$ amounts to 14.6 kJ mol^{-1}.

When this s−o effect is included in the reaction enthalpies at 298 K listed in Table 4, the lowest level MP2 value becomes overestimated. The agreement with experiment improves when more correlation is included (levels I and II) and larger basis sets are used, with the G2 method showing the best agreement, 46.4 kJ mol^{-1} vs 40.4 ± 0.4 kJ mol^{-1} (see also section 6.2 for further discussion).

To present the barrier heights, we list them for the reverse reaction CHClBr + HBr (−1) in Table 4. The reaction between CHClBr and HBr is substantially exothermic and, similarly to the reactions of other carbon-centered free radicals with HBr, possesses small barrier. The computed classical barrier heights show a large scatter ranging from −2.1 to 11.3 kJ mol^{-1}. We give preference, albeit somewhat arbitrarily, to the G2 result (level III). Thus, the barriers for the forward (1) and reverse (−1) reactions are 49.4 and 2.9 kJ mol^{-1}, respectively. The G2 method is preferred because it has been tested and validated to provide reliable saddle point energies for a wide range of reactions.[32,33]

As mentioned, the hydrogen-bridged complexes, RHB and PHB, are true local minima on the PES at the MP2 level. The energy and enthalpy data in Table 4 indicate, however, that the reactants' complex, RHB, may not be stable. The PHB complex, formed between the products, shows stability but just by a few kJ mol^{-1}, and inclusion of ZPE and TC corrections make its energy well even shallower. The small stabilization energies cast doubt on the mere existence of the complex that might be just an artifact due to basis-set superposition error (BSSE). (For a further discussion of the hydrogen bonded complexes see section 6.2.)

The reaction-path analysis has been carried out on data estimated at the MP2/6-31G(d,p) level (energies, gradients, and Hessians). Figure 5 shows the classical energy along the MEP, V_{MEP}, the ground-state vibrationally adiabatic potential energy curve, ΔV_a^G, and the change in the local zero-point energy, ΔZPE, as a function of s over the range −1.0 to +1.0 bohr. Note that the level of zero is at the reactants, Br + CH_2ClBr, for all these functions ($s = -\infty$).

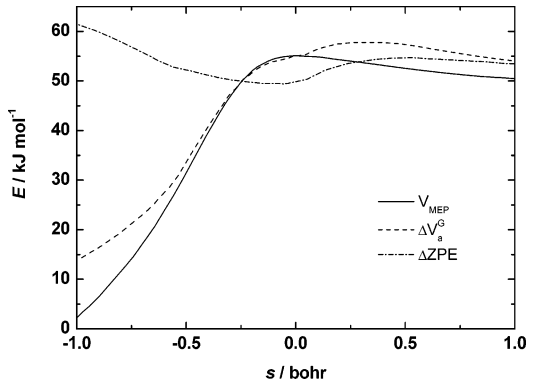

Figure 5. Classical potential energy along the minimal energy path (V_{MEP}), zero-point energy curve (ΔZPE), and ground-state vibrationally adiabatic potential energy curve (ΔV_a^G) with respect to the reactants as a function of the reaction coordinate, s.

In order to improve the energy description of the reaction path at the MP2 level (level 0), higher-level ab initio calculations would be required. However, given that two Br atoms and one Cl atom are involved in this reaction, the use of higher-level ab initio calculations for the complete calculation of the reaction path, and the calculation of the energy second derivatives along the path, are practically prohibitive. Thus, we have used an economical alternative, which has been previously used for other hydrogen abstraction reactions with good results.[53,54] Therefore, in our present case, the alternative to improve the energy description of the reaction is to scale the MP2 results to reproduce the highest level used (G2), employing a factor of

$$F = \Delta E(\text{level 0}, s = 0)/\Delta E(\text{level III}, s = 0)$$

where ΔE is the barrier height at each level. At the saddle point, $s = 0$, the barrier height is that of the highest level, level III. This factor is 0.583.

5.3. Rate Constants for Reactions 1 and −1. In the canonical version of VTST, CVT, the dividing surface is varied along the reaction path to minimize the rate constants, obtaining the generalized transition state (GTS) at the value s*. Thermodynamically, the minimum rate constant criterion is equivalent to maximizing the generalized standard-state free energy of activation, $\Delta G^{\text{GT},\circ}(T,s)$, eq III. Therefore, the effects of the potential energy, entropy, and temperature on the location of this GTS must be considered. In order to make comparisons, we have computed rate constants for both the forward (1) and reverse (−1) reactions by using the classical TST approach, k(TST), and its variational version, k(CVT), and by inclusion of small-curvature tunneling correction, k(CVT/SCT). These rate constants are listed in Table 5 over the temperature range 200−1000 K.

6. Discussion

6.1. Thermochemistry of Reaction 1. The theoretical enthalpy of formation for the CH_2ClBr molecule we used in our derivations (section 4.2: $\Delta_f H°_{298}$ (CH_2ClBr) = −48.1 ± 2.5 kJ mol^{-1} [45]) appears to be the best datum reported in the literature. Published values range from −37.7 kJ mol^{-1} [55] to −45.0 kJ mol^{-1}, where the latter is given by Gurvich et al.[56]

TABLE 5: Comparison of Experimental and Theoretical Rate Constants for the Forward (1) and Reverse (−1) Reactions[a]

T (K)	k(TST)	k(CVT)	k(CVT)/k(TST)	k(CVT/SCT)	k(expt)
		Reaction Br + CH_2ClBr (1)[b]			
200	2.3×10^{-1}	3.0×10^{-2}	0.13	1.0×10^{-1}	
250	1.1×10^{2}	2.2×10^{1}	0.19	4.8×10^{1}	3.2×10^{3}
300	7.8×10^{3}	1.9×10^{3}	0.25	3.3×10^{3}	1.5×10^{5}
350	1.6×10^{5}	4.9×10^{4}	0.30	7.2×10^{4}	2.2×10^{6}
400	1.7×10^{6}	5.8×10^{5}	0.35	7.8×10^{5}	1.7×10^{7}
450	1.1×10^{7}	4.2×10^{6}	0.38	5.2×10^{6}	8.4×10^{7}
500	5.0×10^{7}	2.0×10^{7}	0.41	2.5×10^{7}	3.0×10^{8}
550	1.8×10^{8}	7.8×10^{7}	0.45	9.0×10^{7}	8.5×10^{8}
600	5.2×10^{8}	2.3×10^{8}	0.45	2.7×10^{8}	2.0×10^{9}
650	1.3×10^{9}	6.0×10^{8}	0.45	6.6×10^{8}	4.2×10^{9}
700	3.0×10^{9}	1.4×10^{9}	0.49	1.6×10^{9}	7.9×10^{9}
720	4.0×10^{9}	1.9×10^{9}	0.48	2.1×10^{9}	9.9×10^{9}
750	6.0×10^{9}	3.0×10^{9}	0.50	3.3×10^{9}	1.4×10^{10}
780	9.0×10^{9}	4.5×10^{9}	0.49	4.8×10^{9}	1.8×10^{10}
800	1.1×10^{10}	5.8×10^{9}	0.51	6.0×10^{9}	2.2×10^{10}
1000	8.4×10^{10}	4.5×10^{10}	0.53	4.6×10^{10}	
		Reaction CHClBr + HBr (−1)[c]			
200	1.1×10^{10}	1.4×10^{9}	0.13	4.9×10^{9}	
250	1.7×10^{10}	3.2×10^{9}	0.19	7.2×10^{9}	
300	2.3×10^{10}	5.7×10^{9}	0.25	9.6×10^{9}	1.1×10^{10}
350	2.9×10^{10}	9.0×10^{9}	0.31	1.3×10^{10}	1.8×10^{10}
400	3.6×10^{10}	1.3×10^{10}	0.35	1.7×10^{10}	2.5×10^{10}
450	4.4×10^{10}	1.7×10^{10}	0.38	2.1×10^{10}	3.3×10^{10}
500	5.2×10^{10}	2.1×10^{10}	0.40	2.6×10^{10}	4.1×10^{10}
550	6.0×10^{10}	2.6×10^{10}	0.44	3.1×10^{10}	4.9×10^{10}
600	7.2×10^{10}	3.2×10^{10}	0.45	3.7×10^{10}	5.7×10^{10}
650	8.4×10^{10}	3.9×10^{10}	0.46	4.4×10^{10}	6.4×10^{10}
700	9.6×10^{10}	4.6×10^{10}	0.48	5.1×10^{10}	7.2×10^{10}
750	1.1×10^{11}	5.5×10^{10}	0.51	5.9×10^{10}	7.9×10^{10}
800	1.3×10^{11}	6.6×10^{10}	0.52	6.6×10^{10}	8.6×10^{10}
1000	2.0×10^{11}	1.1×10^{11}	0.55	1.1×10^{11}	

[a] Rate constants are in $cm^3\ mol^{-1}\ s^{-1}$. [b] The experimental rate constants are obtained by the recommended k_1 expression from the current work determined in the temperature range 293−785 K. [c] The experimental rate constants are obtained by the k_{-1} expression reported by Seetula[16] in the temperature range 414−787 K.

NIST Webbook reports (−20 ± 7) kJ mol^{-1} citing Skorobogatov et al.[57] The theoretical enthalpy is preferred because, after a detailed search in the literature, we had been unable to trace back any of the reported experimental values to real experimental (e.g., calorimetric) determinations and the reported data show large scatter; moreover, the computations performed with different high-level methods provided $\Delta_fH°_{298}$ (CH_2ClBr) in good agreement.[45]

The kinetic data determined by us for the forward reaction (1) and those reported by Seetula for the reverse reaction (−1)[16] are both believed to be of high quality that cover a wide temperature range. Both sets of rate constants obey the Arrhenius law and their temperature range overlap in a substantial region even close to room temperature. Therefore, the Arrhenius activation energies determined from the experiments are valid at $T = 298$ K as well. This allows equating the standard reaction enthalpy directly, without the involvement of *any* thermochemical data:

$$\Delta_rH°_{298}(1) = E_{A,1} - E_{A,-1} = (47.6 \pm 0.3) - (8.2 \pm 0.3) = (39.4 \pm 1.0)\ \text{kJ mol}^{-1}$$

The reaction enthalpy thus obtained is in very good agreement with that of the second law derivation in section 4.2, $\Delta_rH°_{298}(1) = (40.4 \pm 0.4)$ kJ mol^{-1}. This good agreement is one of the reasons why we prefer the second law result of $\Delta_fH°_{298}$(CHClBr) = (140.42 ± 2.02) kJ mol^{-1} (section 4.2). In the third law procedure we have calculated $\Delta_fH°_{298}$ (CHClBr) = (136.7 ± 2.8) kJ mol^{-1}, which we believe less accurate because of the likely uncertainties of the entropy values in the calculations. (The uncertainty is reflected by the available standard entropy values of $S°_{298}(CH_2ClBr) = 286.49$[16] and 287.785[56] J mol^{-1} K^{-1} as well as $S°_{298}$(CHClBr) = 294[16] and 291.700[70] J mol^{-1} K^{-1}).

The recommended standard enthalpy of formation of radical CHClBr from our current work is

$$\Delta_fH°_{298}(\text{CHClBr}) = (140 \pm 4)\ \text{kJ mol}^{-1}$$

with a proposed accuracy that is believed to be valid at the 95% confidence level. With this enthalpy of formation the standard reaction enthalpy is $\Delta_rH°_{298}(1) = (40 \pm 4)$ kJ mol^{-1}.

The $\Delta_fH°_{298}$ value we recommend for the CHClBr radical is somewhat lower than the theoretical value of Espinosa-García and Dóbé[45] (146.9 ± 6.3 kJ mol^{-1}) and the experimental estimate of Seetula[16] (143 ± 6 kJ mol^{-1}), but they all agree if their uncertainties are considered.

6.2. Kinetics and Molecular Mechanism of Reaction (1, −1). *Kinetics.* The experimental rate constants for the reaction of Br atoms with CH_2ClBr lie on the same straight line in a ln k_1 vs $1/T$ Arrhenius plot in a wide range of temperatures determined from both relative-rate and absolute kinetics measurements (Figure 4). While such an agreement between the LP and RR results is not expected to be fortuitous, a possible source of systematic errors is worth considering.

All the k_1 values in the lower-temperature regime (between 293 and 583 K) were determined relative to the reference reaction Br + *neo*-C_5H_{12} (2). Thus, any error in k_2 would appear in the rate constant of the studied reaction too. Note that the absolute reaction kinetics studies for reaction 2 were carried out at high temperature ($T = 688-775$ K)[21] and an extrapolation of high-temperature kinetic data to low temperatures is fraught with uncertainties. In order to derive a set of independent k_1 values we have utilized the rate constant expression that we determined in a previous relative-rate kinetic investigation:[58] $k_5/k_1 = (1.6 \pm 0.2)\ \exp[(-15.2 \pm 0.3)\ \text{kJ mol}^{-1}/RT]\ \text{cm}^3\ \text{mol}^{-1}\ \text{s}^{-1}$ ($T = 353-410$ K).

$$\text{Br} + \text{CH}_3\text{Br} \leftrightarrow \text{CH}_2\text{Br} + \text{HBr} \qquad (5, -5)$$

Rate constants for the reverse reaction (−5) are available from absolute kinetic measurements reported in the literature.[16] Taking this kinetic information, and making use of the thermochemistry of reaction 5 with parameters from refs 45 and 59, k_5 is obtained as a function of temperature.[60] Thus, the k_5/k_1 ratio can be resolved to k_1 values that are also plotted in Figure 4 for visualization. The rate constants derived in this way display an excellent agreement with the experimental results from the current work, but they were not included in the estimation of the kinetic parameters.

As far as we are aware, there has been no prior kinetic investigation of reaction 1 either experimentally, apart from our own relative-rate study[58] (see above), or theoretically applying the direct dynamics approach. The experimental and theoretical rate constants from the present work are compared in Table 5 and Figure 6.

Theory predicts significantly smaller rate constants for the reaction Br + CH_2ClBr (1) compared with experiment, and the deviation increases with decreasing temperature as seen, e.g., by the rate constant ratios of k_1(expt)/k_1(CVT/SCT) = 4.2, 21.8, and 45.5 obtained at $T = 750$, 400, and 300 K, respectively.

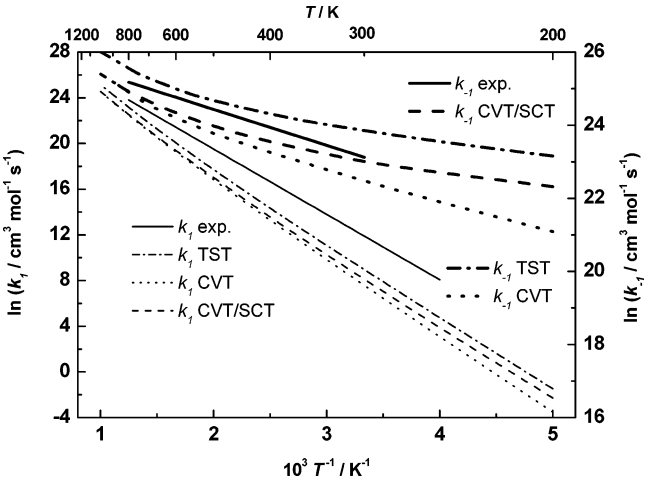

Figure 6. Comparison of experimental and theoretical rate constants for the reactions Br + CH_2ClBr (1) and CHClBr + HBr (−1) (for abbreviations see text).

Moreover, the computed rate constants show a concave upward curvature in ln k_1 vs $1/T$ plots at high temperatures, while the experimental results are described by the simple Arrhenius law in the temperature range studied (see Figure 4). The curvature can be characterized by the phenomenological activation energy of $E_1(\mathrm{CVT/SCT}) = RT^2[\partial \ln k_1(\mathrm{CVT/SCT})/\partial T] = 63.7$ kJ mol^{-1} ($T = 750$ K), which is to be compared with the recommended experimental activation energy of $E_{A,1} = (47.6 \pm 0.3)$ kJ mol^{-1} ($T = 293-785$ K). Some upward curvature of the Arrhenius graph is spotted also by the experimental data determined from the highest temperature studies. The deviation from linearity is, however, small; the activation energy derivable from the LP/RF experiments alone is only ∼3 kJ mol^{-1} larger than the recommended value (see section 4.1).

The reverse reaction CHClBr + HBr (−1), as noted (section 4.2), was studied experimentally by Seetula,[16] who employed the LP/PIMS absolute reaction kinetics method. We have computed rate constants for this reverse reaction as well that are compared with the experimental ones also in Table 5 and Figure 6. The agreement in this case is much better, the rate constant ratios being, for example, $k_{-1}(\mathrm{expt})/k_{-1}(\mathrm{CVT/SCT}) =$ 1.4, 1.5, and 1.5 at $T = 750$, 400, and 300 K, respectively. Importantly, the temperature dependence of the reaction of CHClBr with HBr has been found small, but definitely positive both in the experiments and by our reaction rate theory computations.

While we believe that the above agreement is remarkable, we do not think that our current result has direct implication concerning the debate over the question of "negative activation energies" of the R + HBr reactions (R is hydrocarbon free radical, CH_3, C_2H_5, etc.). This question has come again in the limelight of interest not only for experimentalists[9−12] but also for theoreticians.[13−15] In our opinion, the disparity among the different groups has not been resolved yet: further experimental studies in very wide temperature ranges and preferably using different techniques, as well as very high level quantum chemical and rate theory computations, are required to provide a conclusive answer.

The perplexing result from our current work is that theory agrees on average much better with experimental results for the reverse reaction (−1) than for the forward reaction (1). This may indicate that the thermochemistry in the theory is not correct. All we can state with certainty is, however, that there is an inconsistency in the computed and experimentally estimated thermochemistry of the reaction. At $T = 298$ K the apparent activation energies for the forward and reverse reactions are $E_1(\mathrm{CVT/SCT}) = 57.1$ kJ mol^{-1} and $E_{-1}(\mathrm{CVT/SCT}) = 6.7$ kJ mol^{-1}, respectively. Their difference gives a "second law" standard reaction enthalpy of 50.4 kJ mol^{-1} (this estimation ignores that tunneling effects are present in the theoretical apparent activation energies). This reaction enthalpy is in accordance with that obtained with the G2 theory when s−o effects were taken into account: $\Delta_r H°_{298}(1) = 46.4$ kJ mol^{-1} (see section 5.2). The 50.4 kJ mol^{-1} standard reaction enthalpy, in turn, translates to $\Delta_f H°_{298}(\mathrm{CHClBr}) = 150.4$ kJ mol^{-1}, which agrees well with the result of an independent ab initio computation, $\Delta_f H°_{298}(\mathrm{CHClBr}) = 146.9 \pm 6.3$ kJ mol^{-1},[45] but it is about 10 and 7 kJ mol^{-1} larger than the experimental estimation from the current work and by Seetula,[16] respectively.

The computed k_1(CVT/SCT) rate constants can be brought close to the experimental values by applying a scaling factor of exp(8 kJ mol^{-1}/RT). This may indicate that it is the barrier of the PES that may have been overestimated in computing the rate constant for the reaction of Br atoms with CH_2ClBr. Reduction of the barrier height by 8 kJ mol^{-1} would result, however, in a barrier close to or below zero for the reverse reaction, in disagreement with the activation energy determined experimentally.[16]

We have applied the small-curvature tunneling approach (SCT), contrary to reaction (1, −1) presenting a heavy−light−heavy mass combination that is generally believed to be more adequately treated by using large-curvature tunneling (LCT) methods. Application of the latter method is, however, computationally very demanding (for current improved versions of the LCT method see, e.g., refs 61 and 62). Moreover, the experimental rate constants in Arrhenius plots (see Figure 6) show no curvature, therefore any indication for a significant tunneling effect. It is noted also that an inappropriate tunneling correction would not explain the disparity between experiment and theory since it would affect both the forward and reverse reaction rate constants the same way. An augmented tunneling transmission coefficient would increase the k_1 rate constant, but, at the same time, the k_{-1} rate constant would also increase.

The deviation between the experimentally measured and computed rate constants for the forward Br + CH_2ClBr (1) reaction is the largest at low temperatures. In the low-temperature experiments Br atoms were produced by the photolysis of Br_2. In the photolysis, besides ground-state Br atoms, spin−orbit-excited Br* atoms are also formed. Thus, the formation of Br* may be considered to give rise to an overestimation of the experimental rate constants. The low-temperature photolysis experiments with Br_2 were, however, always carried out in 1.0 bar of He, which greatly facilitated the relaxation of Br* to Br. (The relaxation is known to be fast even with the low collision efficiency He atoms.[63]) Moreover, the stationary concentration of bromine atoms in the photolysis system is thought to be determined essentially by the fast chain-carrier reactions R + Br_2 → RBr + Br (R = CHClBr and *neo*-C_5H_{11}) in which ground-state Br atoms are formed. That is, Br* probably does not play a role in the formation of the photobromination products.

In summary, at present we cannot offer a conclusive reason to explain the deviation between experiment and theory in our current work. The discrepancy can be due to experiment and/or theoretical deficiencies. Further experiments and theoretical studies are required to resolve the disagreement and also to explain why the theoretical Arrhenius plots for k_1 and k_{-1} predict more curvature than determined experimentally.

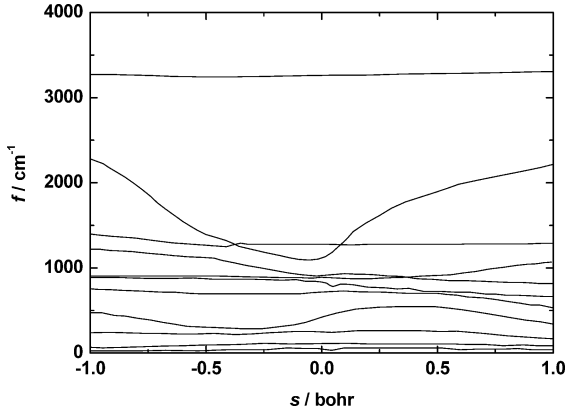

Figure 7. Generalized normal-mode frequencies plotted against the reaction coordinate, *s*. In this figure the 11 real frequencies are presented along the reaction path in the vicinity of the saddle point ($s = 0$). Two of the frequencies disappear in the reactants ($s = -\infty$), and four of them disappear in the products ($s = +\infty$).

Mechanism. The generalized normal mode vibrational analysis as shown in Figure 7, together with the reaction-path analysis in Figure 5, provides insight to some of the dynamic features of the reaction of Br atoms with CH_2ClBr and its reverse, the reaction of CHClBr with HBr. The frequency of the normal mode related to the breaking (C−H)/forming (Br−H) bonds drops dramatically near the saddle point (*reactive mode*). This mode presents a widening of the vibrational well, an effect that has also been found in other reactions with a small skew angle.[64] The two lowest vibrational frequencies along the reaction-path (*transitional modes*) correspond to the transformation of free rotations or free translations into vibrational motions. Their frequencies tend asymptotically to zero at the reactant and product limits showing flat maxima in the saddle point zone. Therefore, the behavior of these transitional modes in the saddle point region only partially compensates the fall in the ZPE caused by the reactive mode, and as a result, the ZPE shows noticeable changes with *s* (Figure 5).

Bottleneck properties of the reaction, determined with the CVT approach, show the location of the generalized transition state to be away from the saddle point, from 0.452 to 0.344 bohr, over the temperature range 200−1000 K. Thus, the variational effects are important, as defined by the ratio of the variational CVT and conventional TST rate constants. As seen in Table 5, the k(CVT)/k(TST) ratios vary between 0.13 and 0.55 in the temperature range between 200 and 1000 K. The variational effect increases with decreasing temperature, and it is the same for the forward and reverse reactions as expected. In the case of the low-barrier reverse reaction (−1), the entropy contribution dominates over the energy contribution, and this is responsible for the variational effect observed.

At mapping the PES of the reaction, we have found two hydrogen bonded complexes at the MP2 level of theory: one in the entrance valley (RHB) and a second one at the product side (PHB). Hydrogen bonded complexes play an important role in the kinetics and dynamics of a great number of reactions as it has been thoroughly presented in recent review articles of the subject.[65,66] This is particularly so for reactions of polar molecules of atmospheric importance,[65,66] but "prereaction" H bonded complexes may affect the kinetics behavior of even large-barrier reactions by increasing the tunneling effect.[67] We believe, however, that one must be cautious when attributing kinetic features to the role of loosely bound molecular complexes that have been estimated at a low theoretical level and are characterized by only small stabilization energy (i.e., if ΔE is less than about 4−6 kJ mol^{-1}). Theoretical scrutiny may reveal such complexes to be just computational artifacts, as that had been shown, e.g., for the reactions $CH_2Br + HBr$[68] and $CH_3Br + HBr$.[14] In the Computational Results section we have already demonstrated that complex RHB is, in reality, unstable. Complex PHB (CHClBr···HBr) appeared to be a real entity by structural and energy results. A possible reason that may give rise to an artificial minimum on the PES is the basis-set superposition error. Thus, we have examined BSSE on complex PHB by using the counterpoise method of Boys and Bernardi.[69] Because of the very high computational cost for the highest levels (I, II, and III) we have calculated the BSSE at level 0 and assumed only 50% of the computed value for the higher levels. With this correction, we conclude that the stability of the PHB complex also disappears at all levels analyzed.

Acknowledgment. This work has been supported by the Hungarian Scientific Research Fund OTKA (Contracts TO37690 and TO43601) as well as the Junta de Extremadura, Spain (Project 2PR-04A001). J.E.-G. gratefully thanks Prof. D. G. Truhlar for providing a copy of the POLYRATE code.

References and Notes

(1) WMO (World Meteorological Organization). *Scientific Assessment of Ozone Depletion: 2002, Global Ozone Research and Monitoring Project*; Report No. 47; World Meteorological Organization: Geneva, 2003; 498 pp.

(2) Rasmussen, R. A.; Khalil, M. A. K. *Geophys. Res. Lett.* **1984**, *11*, 433.

(3) Class, T. H.; Ballschmiter, K. *J. Atmos. Chem.* **1988**, *6*, 35.

(4) Wuebbles, D. J.; Jain, A. K.; Patten, K. O.; Connell, P. S. *Atmos. Environ.* **1998**, *32*, 107.

(5) Kistiakowsky, G. B.; Van Artsdalen, E. R. *J. Chem. Phys.* **1944**, *12*, 469.

(6) McMillen, D. F.; Golden, D. M. *Annu. Rev. Phys. Chem.* **1982**, *33*, 493.

(7) Berkowitz, J.; Ellison, G. B.; Gutman, D. *J. Phys. Chem.* **1994**, *98*, 2788.

(8) Ruscic, B.; Boggs, J. E.; Burcat, A.; Császár, A. G.; Demaison, J.; Janoschek, R.; Martin, J. M. L.; Morton, M. L.; Rossi, M. J.; Stanton, J. F.; Szalay, P. G.; Westmoreland, P. R.; Zabel, F.; Bérces, T. *J. Phys. Chem. Ref. Data* **2005**, *34*, 573.

(9) Seakins, P. W.; Pilling, M. J.; Niiranen, J. T.; Gutman, D.; Krasnoperov, L. A. *J. Phys. Chem.* **1992**, *96*, 9847.

(10) Dobis, O.; Benson, S. W. *J. Phys. Chem. A* **1997**, *101*, 6030.

(11) Benson, S. W.; Dobis, O. *J. Phys. Chem.* **1998**, *102*, 5175.

(12) Krasnoperov, L. N.; Mehta, *K. J. Phys. Chem. A* **1999**, *103*, 8008.

(13) Yu, H. G.; Nyman, *G. J. Phys. Chem. A* **2001**, *105*, 2240.

(14) Espinosa-García, J. *J. Chem. Phys.* **2002**, *117*, 2076.

(15) Sheng, L.; Li, Z. S.; Liu, J. Y.; Sun, C. C. *J. Chem. Phys.* **2003**, *119*, 10585.

(16) Seetula, J. A. *Phys. Chem. Chem. Phys.* **2003**, *5*, 849.

(17) Baldridge, K. M.; Gordon, M. S.; Steckler, R.; Truhlar, D. G. *J. Phys. Chem.* **1989**, *93*, 5107.

(18) Espinosa-García, J.; Corchado, J. C.; Truhlar, D. G. *J. Am. Chem. Soc.* **1997**, *119*, 9891.

(19) Villá, J.; González-Lafont, A.; Lluch, J. M.; Corchado, J. C.; Espinosa-García, J. *J. Chem. Phys.* **1997**, *107*, 7266.

(20) Dóbé, S.; Bérces T.; Turányi T.; Márta, F.; Grussdorf, J.; Temps, F.; Wagner, H. Gg. *J. Phys. Chem.* **1996**, *100*, 19864.

(21) Imrik, K.; Dóbé, S.; Bérces, T. *Int. J. Chem. Kinet.* **2001**, *33*, 49.

(22) Fettis, G. C.; Knox, J. H.; Trotman-Dickenson, A. F. *J. Chem. Soc.* **1960**, 4177.

(23) Miyokawa, K.; Tschuikow-Roux, E. *J. Phys. Chem.* **1990**, *94*, 715.

(24) Bierbach, A.; Barnes, I.; Becker, K. H. *Int. J. Chem. Kinet.* **1996**, *28*, 565.

(25) Frisch, M. J.; Trucks, G. W.; Schlegel, H. B.; Scuseria, E.; Robb, M. A.; Cheeseman, J. R.; Zakrzewski, V. G.; Montgomery, J. A.; Stratman, R. E.; Burant, J. C.; Dapprich, S.; Millam, J. M.; Daniels, A. D.; Kudin, K. N.; Strain, M. C.; Farkas, O.; Tomasi, J.; Barone, V.; Cossi, M.; Cammi, R.; Menucci, B.; Pomelli, C.; Adamo, C.; Clifford, S.; Ochterki, J.; Petterson, G. A.; Ayala, P. Y.; Cui, Q.; Morokuma, K.; Malik, D. K.; Rabuk, A. D.; Raghavachari, K.; Foresman, J. B.; Cioslowski, J.; Ortiz, J. V.; Stefanov, J. J.; Liu, G.; Liashenko, A.; Piskorz, P.; Komaromi, I.; Gomperts, R.; Martin, R. L.; Fox, D. J.; Keith, T.; Al-Laham, M. A.; Peng, C. Y.; Nanayakkara, A.; González, C.; Challacombe, M.; Gill, P. M. W.; Johnson,

B. G.; Chen, W.; Wong, M. W.; Andres, J. L.; Head-Gordon, M.; Reploge, E. S.; Pople, J. A. *Gaussian 98*, revision A. 7; Gaussian Inc.: Pittsburgh, PA, 1998.

(26) Møller, C.; Plesset, M. S. *Mol. Phys.* **1934**, *46*, 618.

(27) Isaacson, A. D.; Truhlar, D. G. *J. Chem. Phys.* **1982**, *76*, 1380.

(28) Raghavachari, K. *J. Chem. Phys.* **1985**, *82*, 4607.

(29) Nobes, R. M.; Pople, J. A.; Radom, L.; Handy, N. C.; Knowles, P. L. *Chem. Phys. Lett.* **1987**, *138*, 481.

(30) Bartlett, R. J. *J. Phys. Chem.* **1989**, *93*, 1697.

(31) Curtiss, L. A.; Raghavachari, K.; Trucks, G. W.; Pople, J. A. *J. Chem. Phys.* **1991**, *94*, 7221.

(32) Ma, N. L.; Smith, B. J.; Pople, J. A.; Radom, L. *J. Am. Chem. Soc.* **1991**, *113*, 7903.

(33) Durant, J. L.; Rohlfing, C. M. *J. Chem. Phys.* **1993**, *98*, 8031.

(34) Miller, W. H.; Handy, N. C.; Adams, J. E. *J. Chem. Phys*. **1980**, *72*, 99.

(35) Morokuma, K.; Kato, S. In *Potential Energy Surfaces and Dynamics Calculations*; Truhlar, D. G., Ed.; Plenum: New York, 1981; p 243.

(36) Kraka, E.; Dunning, T. H. In *Advances in Molecular Electronic Structure Theory*; JAI: New York, 1990; Vol. I, p 129.

(37) Garrett, B. C.; Truhlar, D. G. *J. Am. Chem. Soc*. **1979**, *101*, 4534.

(38) Truhlar, D. G.; Isaacson, A. D.; Garrett, B. C. In *The Theory of Chemical Reactions*; Baer, M., Ed.; Chemical Rubber: Boca Raton, FL, 1985; Vol. 4.

(39) Lu, D. h.; Truong, T. N.; Melissas, V. S.; Lynch, G. C.; Liu, Y. P.; Garrett, B. C.; Steckler, R.; Isaacson, A. D.; Rai, S. N.; Hancock, G. C.; Lauderdale, G. C.; Joseph, T.; Truhlar, D. G. *Comput. Phys. Commun*. **1992**, *71*, 235.

(40) Chuang, Y. Y.; Corchado, J. C.; Fast, P. L.; Villá, J.; Coitiño, E. L.; Hu, W. P.; Liu, Y. P.; Lynch, G. C.; Nguyen, K.; Jackells, C. F.; Gu, M. Z.; Rossi, I.; Clayton, S.; Melissas, V.; Steckler, R.; Garrett, B. C.; Isaacson, A. D.; Truhlar, D. G. *POLYRATE*, version 8.4; University of Minnesota: Minneapolis, 1999.

(41) McGivern, W. S.; Li, R.; Zou, P.; North, S. W. *J. Chem. Phys.* **1999**, *111*, 5771.

(42) Timonen, R. S.; Seetula, J. A.; Gutman, D. *J. Phys. Chem.* **1990**, *94*, 3005.

(43) Timonen, R. S.; Seetula, J. A.; Niiranen, J. J.; Gutman, D. *J. Phys. Chem.* **1991**, *95*, 4009.

(44) Enthalpy increments: $[H°_{600} - H°_{298}](\mathrm{Br}) = 6.239$ kJ mol^{-1} and $[H°_{600} - H°_{298}](\mathrm{HBr}) = 8.814$ kJ mol^{-1} from ref 59; $[H°_{600} - H°_{298}](\mathrm{CHClBr}) = 15.707$ kJ mol^{-1} from ref 70; and $[H°_{600} - H°_{298}](\mathrm{CH_2ClBr}) = 19.296$ kJ mol^{-1} from ref 56. Auxiliary enthalpies of formation: $\Delta_f H°_{298}(\mathrm{Br}) = 111.87 \pm 0.12$ kJ mol^{-1} and $\Delta_f H°_{298}(\mathrm{HBr}) = -36.29 \pm 0.16$ kJ mol^{-1} from ref 59.

(45) Espinosa-García, J.; Dóbé, S. *J. Phys. Chem. A* **1999**, *103*, 6387.

(46) Auxiliary entropy values: $S°_{600}(\mathrm{Br}) = 189.451$ J K^{-1} mol^{-1} and $S°_{600}(\mathrm{HBr}) = 219.108$ J K^{-1} mol^{-1} from ref 59; $S°_{600}(\mathrm{CH_2ClBr}) = 331.362$ J K^{-1} mol^{-1} from ref 56; and $S°_{600}(\mathrm{CHClBr}) = 333.377$ J K^{-1} mol^{-1} from MP2/6-31G(d,p) calculations of Espinosa-García, ref 70.

(47) Hehre, W. J.; Radom, L.; Schleyer, P. R.; Pople, J. A. *Ab initio Molecular Orbital Theory*; Wiley: New York, 1989; p 228.

(48) *JANAF Thermochemical Tables*, 3rd ed.; Chase, M. W., Davies, C. A., Downey, J. R., Frurip, D. J., McDonald, R. A., Syverud, A. N., Eds.; National Standard Reference Data Series 14; National Bureau of Standards: Washington, DC, 1985.

(49) Jacox, M. E. *J. Phys. Chem. Ref. Data* **1984**, *13*, 945.

(50) Pyykkö, P. *Chem. Rev.* **1988**, *88*, 563.

(51) Peterson, K. A.; Kendall, R. A.; Dunning, T. H. *J. Chem. Phys.* **1993**, *99*, 1930.

(52) Martin, J. M. L.; Taylor, P. R. *J. Phys. Chem.* **1998**, *102*, 2995.

(53) Espinosa-García, J.; Corchado, J. C. *J. Chem. Phys*. **1994**, *101*, 8700.

(54) Espinosa-García, J. *J. Phys. Chem*. *A* **2000**, *104*, 7537.

(55) Bernstein, H. J. *J. Phys. Chem.* **1965**, *69*, 1550.

(56) Gurvich, L. V.; Veyts, I. V.; Alcock, C. B. *Thermodynamic Properties of Individual Substances*, 4th ed; Hemisphere: New York, 1991; Vol. 2, Part 2.

(57) Skorobogatov, G. A.; Dymov, B. P.; Nedozrelova, I. V. *Russ. J. Gen. Chem. (Engl. Transl.)* **1996**, *66*, 1777.

(58) Imrik, K.; Sarzyñski, D.; Dóbé, S.; Bérces T.; Márta, F. *React. Kinet. Catal. Lett.* **2003**, *78*, 309.

(59) Cox, J. D.; Wagman, D. D.; Medvedev, V. A. *CODATA Key Values for Thermodynamics*; Hemisphere: New York, 1989; see also http://www.codata.org/codata/databases/key1.html.

(60) Imrik, K. Unpublished results.

(61) Fernández-Ramos, A.; Truhlar, D. G. *J. Chem. Phys.* **2001**, *114*, 1491.

(62) Fernández-Ramos, A.; Truhlar, D. G.; Gorchado, J. C.; Espinosa-García, J. *J. Phys. Chem.* **2002**, *106*, 4957.

(63) Donovan, R. J.; Husain, D. *Trans. Faraday Soc.* **1966**, *62*, 2987.

(64) Bondi, D. K.; Connor, J. N. L.; Garrett, B. C.; Truhlar, D. G. *J. Chem. Phys*. **1983**, *78*, 5981.

(65) Smith, I. W.; Ravishankara, A. R. *J. Phys. Chem. A* **2002**, *106*, 4798.

(66) Hansen, J. C.; Francisco, J. S. *Chem. Phys. Chem*. **2002**, *3*, 833.

(67) Masgrau, L.; González-Lafont, À.; Lluch, J. M. *J. Comput. Chem.* **1999**, *20*, 1685.

(68) Espinosa-García, J. *Mol. Phys.* **1999**, *97*, 629.

(69) Boys, S. F.; Bernardi, F. *Mol. Phys.* **1970**, *19*, 553.

(70) Espinosa-García, J. unpublished results from MP2/6-31G(d,p) calculations; a list of the calculated thermodynamic properties is available from the authors on request.

(71) *Numerical Data and Functional Relationships in Science and Technology*; Hellwege, K. H., Hellwege, A. M., Eds.; Springer-Verlag: Berlin, 1987; Vol. 15 (supplement to Vol. II-17).